Mid- and long-chain leaf waxes and their δ^2H signatures in modern plants and lake sediments from mid-latitude North America

Ioana C. Stefanescu[1*], Chandelle Macdonald[2], Craig S. Cook[2], David G. Williams,[2,3] Bryan N. Shuman[1]

[1]Department of Geology and Geophysics, University of Wyoming, Laramie, WY, USA

[2]The Stable Isotope Facility, University of Wyoming, Laramie, WY, USA

[3]Department of Botany, University of Wyoming, Laramie, WY, USA

***Corresponding author:**

1000 E University Ave., Science Initiative Bldg. Room 4234, Laramie, WY, 82071, USA

E-mail address: istefane@uwyo.edu (Ioana C. Stefanescu)

Keywords: Stable isotopes, leaf-waxes, hydroclimate reconstructions

Abstract

Compound-specific δ^2H composition of leaf-wax n-alkanes are increasingly being used to infer past hydroclimates. However, differences in n-alkane production and apparent fractionation factors (ε_{app}) among different plant groups complicate the relationships between n-alkane and environmental water δ^2H. Mid- and long-chain n-alkanes in sedimentary archives (i.e., C_{23} and C_{29}) are thought to derive from aquatic and terrestrial plants, respectively, and track the isotopic composition of either lake water or precipitation. Yet, the relationship between the δ^2H composition of alkane C_{23} and that of lake water is not well constrained. Moreover, recent studies show that n-alkane production is greater in terrestrial plants than in aquatic plants, which has the potential to obscure n-alkane aquatic inputs to sedimentary archives. Here, we investigated n-alkane contributions to sedimentary archives from both aquatic and terrestrial plants by analyzing their distributions and δ^2H signatures in plants and lake sediments at 29 sites across mid-latitude North America. We find that both aquatic and terrestrial plants synthesize alkane C_{23} and that sedimentary C_{23} δ^2H values parallel those of terrestrial plants and differ from those of aquatic plants. Our results indicate that across mid-latitude North America, and globally, both mid- and long-chain n-alkanes in lake sediments commonly derive from terrestrial higher plants challenging the assumption that submerged aquatic plants produce the C_{23} alkane preserved in lake sediments. Moreover, angiosperms and gymnosperms exhibit similar ε_{app} values between the δ^2H of alkane C_{29} and mean annual precipitation. Therefore, vegetation shifts between angiosperms and gymnosperms do not strongly affect the ε_{app} between alkane C_{29} and MAP. Our results show that both mid- and long-chain alkanes track the isotopic composition of mean annual precipitation in the temperate region of North America.

1. Introduction

Compound-specific hydrogen isotopic ratios of leaf-wax n-alkanes are increasingly being used as proxies for past precipitation changes (Schefuß et al., 2005; Pagani et al., 2006; Tierney et al., 2008; Aichner et al., 2010a; Tierney et al., 2011; Rach et al., 2014; Curtin et al., 2019; Puleo et al., 2020). Leaf wax n-alkanes are simple, unbranched, long-chain H saturated organic compounds (formula: C_nH_{2n+2}) biosynthesized by plants at the leaf surface during leaf formation from alkanoic acids through the decarboxylation pathway (Jetter et al., 2006; Sachse et al., 2010; Tipple et al., 2013). A stable chemical configuration enables n-alkanes to preserve well in marine and freshwater sediments and facilitates extraction and purification (Yang and Huang, 2003; Sessions et al., 2004; Schimmelmann et al., 2006; Diefendorf et al., 2015; Sessions, 2016). Depending on the plant growth environment, the hydrogen source of leaf-wax n-alkanes may derive from canopy-intercepted precipitation, soil moisture, or lake water. Since precipitation is the ultimate hydrogen source of soil moisture and lake water, leaf-wax n-alkanes have been shown to track the hydrogen isotopic signature of precipitation and have become instrumental for studying past changes in environmental moisture (Sachse et al., 2004; Sachse et al., 2012; Tipple et al., 2013, McFarlin et al., 2019). Because different compounds may represent different moisture sources (e.g., lake water versus soil moisture), understanding the differences could further enhance reconstruction of multiple hydrologic processes such as soil or lake evaporation (Rach et al., 2014; Rach et al., 2017; Curtin et al., 2019).

The abundance of n-alkanes in leaf-waxes and the relative abundances of the different chain lengths varies widely between plant types and between different environments (Ficken et al., 2000; Diefendorf et al., 2011; Feakins et al., 2016; Liu and Liu, 2016; Liu et al., 2017). For example, terrestrial broad leaf trees produce up to 300 times more n-alkanes than shrubs and

grasses (Freimuth et al., 2019), n-alkanes are up to 200 times more abundant in angiosperms than in gymnosperms (Diefendorf et al., 2011), and 30 times more abundant in terrestrial than aquatic plants (Dion-Kirschner et al., 2020). The distribution of n-alkane chain lengths also varies based on plant growth environment. Aquatic submerged plants preferentially produce mid-chain homologues (C_{21}-C_{25}) (Fiken et al., 2000, Aichner et al., 2010b; Gao et al., 2011), while terrestrial plants maximally form long-chain homologues (>n-C_{25}) (Bush and McInerney, 2013). The difference in the most common chain lengths between aquatic and terrestrial plants has led to the use of the mid-chain alkane C_{23} as proxy for lake water δ^2H and evapotranspiration (Ficken et al., 2000; Seki et al., 2011; Rach et al., 2014; Rach et al., 2017; Curtin et al., 2019; Puleo et al., 2020) and to the use of the long-chain alkane C_{29} as proxy for precipitation δ^2H (Sachse et al., 2004; Sachse et al., 2012; McFarlin et al., 2019). A challenge with this approach has been that most plants produce varying amounts of both mid- and long-chain n-alkanes (Ficken et al., 2000; Gao et al., 2011; Feakins et al., 2016; Wang et al., 2018; Dion-Kirschner et al., 2020; He et al., 2020), and the high production rates of all n-alkanes by terrestrial plants may dominate over aquatic sources even for mid-chain lengths (Freimuth et al., 2019).

Precipitation δ^2H composition undergoes isotopic fractionation through soil or lake water evaporation as well as during plant biosynthesis, which leads to a systematic difference between the δ^2H of n-alkanes relative to that of precipitation. This apparent fractionation factor (ε_{app}) varies as a function of chain length, as well as plant type, climatic conditions and geographic location (Sachse et al., 2012; Feakins et al., 2018; McFarlin et al., 2019). The ε_{app} has been well described for the C_{29} n-alkane, enabling estimates of precipitation δ^2H (Sachse et al., 2012; McFarlin et al., 2019). A recent global compilation of leaf-wax δ^2H from sedimentary archives

(McFarlin et al., 2019) confirmed a strong relationship (r^2=0.8) between the δ^2H of alkane C_{29} and mean annual precipitation (MAP) with an average apparent fractionation factor, $\varepsilon_{C29/MAP}$, of -121‰ (s.d.=18 ‰). However, ε_{app} for alkane C_{23} relative to lake water δ^2H has not been as widely constrained; the relationship (r^2=0.4) is much weaker than for C_{29} and MAP (McFarlin et al., 2019). Consequently, although the δ^2H values of alkanes C_{29} and C_{23} are assumed to represent terrestrial and aquatic sources, and often treated as $\delta^2H_{Terrestrial}$ and $\delta^2H_{Aquatic}$, respectively (Rach et al., 2014), these relationships may be complex in many settings (McFarlin et al., 2019; Dion-Kirschner et al., 2020; He et al., 2020).

Models have been developed to differentiate the n-alkane sources (i.e., aquatic or terrestrial inputs) in sedimentary archives based on the relative abundances of mid- and long-chain n-alkanes (Fiken et al., 2000; Gao et al, 2011; Wang et al., 2018, Dion-Kirschner et at., 2020, Peaple et al., 2021). However, differences in n-alkane production between terrestrial and aquatic plants combined with different plant distributions in and around lakes presents a challenge to this approach (Diefendorf and Freimuth, 2017). Aquatic n-alkane input to sediments might be important and therefore distinguishable in low latitude environments due to a year-round growing season (Mead et al., 2005), but biosynthesis of aquatic n-alkanes is limited to a growing season at mid- and high-latitudes, where even alkane C_{23} input to sedimentary archives might be dominated by terrestrial sources. A recent study from Greenland shows that leaf-wax distributions and n-alkane δ^2H values in sedimentary archives are more similar to those observed in terrestrial plants, and, therefore, mid-chain n-alkanes do not track lake water isotopic signatures at high latitudes (Dion-Kirschner et al., 2020).

Given the need to elucidate the use of alkane C_{23} as a proxy for lake water δ^2H values in temperate regions, we analyze the distributions and δ^2H composition of mid- and long-chain n-

alkanes in sediments, aquatic plants, and terrestrial plants across mid-latitude North America. We investigate the potential leaf-wax sources in lake sediments from the Rocky Mountains east to the Atlantic coast and evaluate the relationships between the δ^2H values of mid- and long-chain n-alkanes and environmental waters.

2. Methods

2.1 Study sites and sample collection

Modern surface sediments, lake water, aquatic and terrestrial plants were collected in and around 29 lakes across the central and eastern United States during May and early June of 2018 (Figure 1, Table 1). The lakes span a large climatic gradient where mean annual air temperatures (MAAT) range from 5.4 to 19.5 ºC. Mean annual precipitation (MAP) varies from 353-1431 mm/year and elevation from 11 to 2181 meters (Table 1). MAAT and MAP were obtained using the Parameter-Elevation Regressions on Independent Slopes Model (PRISM) with a resolution of 800 meters from the Climate Group at Oregon State University (Prism Climate Group, 2019). The lakes are surrounded by both tree and graminoid angiosperms, but gymnosperms trees also grow near some of the lakes (see data file). Leaves were collected from aquatic angiosperm plants in 19 of the lakes, from angiosperms trees at 29 sites, from gymnosperms trees at 12 sites, and from grasses at 26 sites.

Modern sediment samples were collected in polycarbonate tubes using a gravity corer at lake depths between 0.3 and 6 meters, and the upper 1 cm of sediment was preserved for n-alkane analysis. We also analyzed a surface sediment sample from Libby Flats Lake, Wyoming, located within sub-alpine meadows and gymnosperm forests and which is part of a network of lakes were lake water isotopic values have been closely monitored (Liefert et al., 2019). Lake water was collected in 60 mL polypropylene bottles. Aquatic and terrestrial leaves were collected and

126 placed in Whirl-Pack bags. Terrestrial leaves were collected from trees and grasses adjacent to
127 the lakes and tree leaves were sampled at a height of ~ 2 meters above ground. All samples were
128 immediately stored at 4 ºC. Sediments and plants were freeze-dried upon arrival at the University
129 of Wyoming. We analyzed the distributions of n-alkanes C_{17}-C_{29} and the δ^2H isotopic ratios of n-
130 alkanes C_{23}-C_{29} in 30 surface sediment samples and 129 plants.

131 **2.2 Plant identification and classification**

132 Plants were identified based on vegetative morphologies and differentiated into major
133 taxonomic groups. Out of the 129 samples (2-10 leaves per plant- depending on leaf size and 10-
134 50 grams of algae), 69 were collected from angiosperm trees, 12 from gymnosperm trees, 26
135 from C3 graminoids (hereafter grasses), and 21 from aquatic macrophytes. The aquatic
136 macrophytes were further divided into subgroups based on their growth habitat within the lake
137 as: algae (n=4), aquatic submergent (n=3), aquatic floating (n=4) and aquatic emergent (n=9).

138 **2.3 Alkane analysis**

139 Lipids were extracted from 2-8 g of freeze-dried sediment and 2-8 g of freeze-dried leaves
140 using an accelerated solvent extractor (ASE Dionex 350) with dichloromethane (DCM):
141 methanol (9:1, volume:volume, hereafter V/V). The total lipid extract was separated over
142 aminopropyl (LC-NH2) solid phase columns using DCM: Isopropanol (2:1, V/V) then re-
143 dissolved in hexane and separated over silica gel columns using hexane to isolate the aliphatic
144 fraction. The aliphatic fraction was re-dissolved in hexane and separated over activated 10%
145 silver nitrate-impregnated silica gel columns to isolate the saturated n-alkane compounds.

146 N-alkane δ^2H was measured by injecting 1μL of the saturated fraction into a Thermo
147 Scientific Trace GC Ultra fitted with an Agilent DB5 column and coupled to a Thermo Delta V

IRMS. The injector was held at a constant temperature of 250 ºC and the reactor at a constant temperature of 1420 ºC. The GC oven was held at 35 ºC for 2 minutes then ramped 3 0ºC/min to a temperature of 225 ºC, held for 1 min, then ramped again 10 ºC/min to a final temperature of 300 ºC and held for 12 minutes. All samples were run in duplicate. A standard n-alkane mixture (mixture A7 from Arndt Schimmelmann, Indiana University) containing alkanes C_{17}-C_{29} was used to identify the n-alkane compounds based on retention times, and to account for instrument D/H offset. We only report the δ^2H values of n-alkanes with amplitudes >1 volt. All δ^2H measurements are reported as per mil (‰) relative to the Vienna Standard Mean Ocean Water (VSMOW). The average H3 factor for all runs was 2.19 and ranged between 1.98 to 2.21 across all runs. Duplicate sample δ^2H measurements were averaged, and the average δ^2H difference between duplicates was 2.4 ‰ across all runs.

We only report the δ^2H values of alkanes C_{23} through C_{29} as the concentrations of short chain alkanes C_{17}-C_{21} in most sediments and terrestrial plants were too low to reliably be measured for the δ^2H isotopic composition.

2.4 Lake water analysis and modeled precipitation data

Lake water samples were analyzed for δ^2H and $\delta^{18}O$ using 12 sequential replicate measurements on a Picarro L2130 isotope analyzer at the Stable Isotope Facility at the University of Wyoming. We report the average δ^2H (‰) and $\delta^{18}O$ (‰) values of the last 3 of the 12 replicate measurements for each lake water sample. The quality control water (UWSIF 303) long-term averages of standard deviation are 1 ‰ for δ^2H and 0.3 ‰ for $\delta^{18}O$.

Modeled monthly and MAP δ^2H values were obtained using the Online Isotopes of Precipitation Calculator (OIPC) (Bowen, G. J., 2020). Seasonal precipitation δ^2H values were

estimated by averaging monthly predicted δ^2H values as follows: Winter- December, January, February (DJF); Spring- March, April, May (MAM); Summer- June, July, August (JJA); and Autumn- September, October, November (SON). Predicted δ^2H values are reported relative to VSMOW.

2.5 Mathematical analysis and notations

For comparison with our results, the global meteoric water line (GMWL, Figure 2) was calculated as in Eq.1 (Craig, 1961):

$$\delta^2H \text{ ‰} = 8 * \delta^{18}O \text{ ‰} + 10 \text{ ‰} \quad (1)$$

N-alkane peak areas were normalized using the A7 standard to account for the loss in peak area associated with GC-IRMS analyses. In short, the equal concentration of all the individual n-alkanes in the A7 standard of 0.701 mg/0.5 mL should yield equal peak areas for each n-alkane when analyzed on the GC-IRMS. However, in GC-IRMS analyses, peak area decreases with increasing chain-length. Therefore, we used the peak area of the first eluting odd alkane, alkane C_{17} in the A7 standard, to normalize the peak areas for the other n-alkanes in the standard. We first calculated the fractional decrease in peak areas for individual n-alkanes relative to the peak area of alkane C_{17}. We then normalized the peak areas in our samples based on the observed decrease in n-alkanes peak areas relative to alkane C_{17} in the A7 standard.

Fractional abundances of individual n-alkanes were then calculated using the normalized peak areas of individual n-alkanes as in Eq.2:

$$f_i = \frac{A_i}{A_{C17} + A_{C19} + A_{C21} + A_{C23} + A_{C25} + A_{C27} + A_{C29}} \quad (2)$$

where *f* is the fraction of individual n-alkanes, *i* varies from C_{17} to C_{29} and *A* signifies peak area.

191 The apparent fractionation (ε_{app}) between leaf wax n-alkanes (from sediments or plants) and
192 source water (e.g., lake water or MAP) was calculated using Eq. 3:

193 $$\varepsilon_{wax/water} = 1000 * (\frac{\delta^2H_{wax} + 1000}{\delta^2H_{water} + 1000} - 1) \quad (3)$$

194 All of our statistical treatments of the data were completed using base functions in R (R Core
195 Team, 2018).

196 **3. Results**

197 **3.1 Modeled MAP and measured lake water δ^2H values**

198 The modeled δ^2H and $\delta^{18}O$ of MAP at our sample sites plot along the GMWL and range
199 from -118 ‰ to -21 ‰ and -16.3 ‰ to -4 ‰, respectively (Figure 2A, Table 1). The measured
200 lake water δ^2H and $\delta^{18}O$ also plot along or near the GMWL but range from -125 ‰ to 3 ‰ and -
201 17 ‰ to 1.8 ‰ respectively, consistent with evaporative enrichment at some lakes and
202 groundwater input or selective winter lake recharge at others (Figure 2B, Table 1). Furthermore,
203 modeled MAP and measured lake water δ^2H values are highly correlated across sites (Pearson's
204 correlation coefficient, r=0.87, p=<0.05) with an average $\varepsilon_{Lake/MAP}$ value of 10 ‰ (Figure 2B).

205 Measured lake water δ^2H correlated more with MAP δ^2H (Pearson's r=0.92, p=<0.05) than
206 with the seasonal values. Consequently, we use MAP δ^2H as the variable of interest in our
207 subsequent analyses. Seasonally, measured lake water δ^2H best correlated with the modelled δ^2H
208 of MAM precipitation (Table 2, Pearson's r=0.88, p<0.05). The modeled δ^2H of MAP also
209 correlated best with the modeled seasonal δ^2H (Table 2) in Spring (MAM, Pearson's r=0.97,
210 p<0.05).

211 **3.2 N-alkane distributions in plants and sediments**

The fractional abundance distributions of the C_{17}-C_{29} n-alkanes in plants and sediments (Figure 3) show that terrestrial plants and sediments maximally yield C_{29} while aquatic plants produced different alkanes dependent on growth type. The n-alkane distribution in angiosperms trees maximizes on alkane C_{29} followed by alkane C_{27}, alkane C_{25} and alkane C_{23}. Gymnosperm trees produced a similar pattern, dominated by alkane C_{29}, but the abundances of the mid-chain alkane C_{23} and the long-chain n-alkanes are more evenly distributed compared to those of angiosperms trees. The short-chain n-alkanes (C_{17}, C_{19} and C_{21}) in both angiosperms and gymnosperms trees exhibit low fractional abundances (mean <0.03). The n-alkane distribution in grasses follow the same pattern as other angiosperm trees, although the fractional abundances of alkane C_{21} is slightly higher in grasses (mean <0.04) than in angiosperm or gymnosperm trees (mean <0.01).

Aquatic algae produce high relative abundances of alkane C_{17} in combination with abundant C_{23}, C_{27}, and C_{29} (top right, Figure 3), while the fractional abundances of alkanes C_{19}, C_{21} and C_{25} are all low (mean <0.07). In submerged plants, the relative abundance of alkane C_{23} exceeds that of the other compounds, although C_{25}, C_{27} and C_{29} are also abundant (mean >0.1). Conversely, the n-alkane distributions in floating and emergent aquatic plants follow a similar distribution to that observed in terrestrial angiosperm trees and grasses with fractional abundances increasing with chain length.

Sediments also contain the same distribution pattern as observed in higher terrestrial trees and grasses or in floating and emergent aquatic plants. Fractional abundances of n-alkanes increase with increasing chain-length in our sediment samples (bottom left, Figure 3), albeit with more C_{23} than may be expected from angiosperm terrestrial plants alone.

3.3 Vegetation effects on sediment n-alkane distributions and δ^2H

Across different regions, and through time, vegetation changes might affect leaf-wax δ^2H values preserved in lake sediments due to differences in the apparent fractionation factors between major plant groups (i.e., angiosperm trees vs. gymnosperm trees). Insight into the potential outcomes are exemplified by sediments from two distinct sites (red symbols, Figure 1): an angiosperm tree dominated site, Libby Flats Lake, versus a gymnosperm tree dominated site, Lake T2L17 (Figure 4). The n-alkane distributions of the sediment from the two sites differed distinctly. The angiosperm site dominated by alkane C_{29}, has low abundance of C_{23}, and little to no C_{17}, C_{19} and or C_{21} (Figure 4A). At the gymnosperm site, alkane $C_{21\text{-}27}$ dominated with alkane C_{29} expressing the lowest abundance of the long-chain n-alkanes. Despite these differences, emblematic of angiosperm versus gymnosperm sources, the apparent fractionation between alkane C_{29} and MAP is similar: $\varepsilon_{C29/MAP}$ is -126 ‰ and -122 ‰ (±2.4 ‰) for the angiosperm and gymnosperm sites, respectively (Figure 4B). Both fall within the range of reported global sedimentary $\varepsilon_{C29/MAP}$ values of -121±18 ‰ (McFarlin et al., 2019).

3.4 Apparent fractionation factors across plant groups and sediments

We calculated the apparent fractionation factors between the δ^2H values of n-alkanes integrated in the surface sediments and those of MAP but also between the δ^2H values of n-alkanes in individual plants and those of MAP (Figure 5; Table 3). The apparent fractionation ($\varepsilon_{alkane/MAP}$) between MAP and alkanes C_{23} to C_{29} in sediments and different plant groups vary, but estimates based on alkanes from sediment and terrestrial plants overlap (Figure 5; Table 3). For both mid- and long-chain alkanes, $\varepsilon_{alkane/MAP}$ distributions are similar for sediments and angiosperm plant samples; the means fell within 1 ‰, 6 ‰, 0 ‰, and 4 ‰ for C_{29}, C_{27}, C_{25} and C_{23}, respectively (Figure 5). Gymnosperm $\varepsilon_{alkane/MAP}$ distributions are similar to those of

sediments for the C_{29} and C_{23} alkanes (within 1 ‰ and 5 ‰, respectively), but lower than those of sediments for the C_{27} and C_{25} alkanes.

Mean $\varepsilon_{alkane/MAP}$ for grasses, however, are consistently lower than for sediments, angiosperm trees, and gymnosperm trees (Figure 5). Mean $\varepsilon_{alkane/MAP}$ is also lower for all aquatic plant groups than for sediments (by 16-51 ‰) with most of aquatic $\varepsilon_{alkane/MAP}$ distributions plotting below the means for $\varepsilon_{alkane/MAP}$ sediments (Figure 5). Even though the water source of aquatic plants is lake water, mean $\varepsilon_{alkane/lake}$ for aquatic plant alkanes versus lake water is also consistently lower than those of sediments (Table 3). Due to low abundances of alkanes C_{23} and C_{25} in floating plants, we were unable to reliably calculate their $\varepsilon_{alkane/MAP}$ distributions.

3.5 Sources of C_{23} and C_{29} alkanes in sediments

Differences in δ^2H between alkanes C_{23} and C_{29}, represented by $\varepsilon_{C29/C23}$, differ among sources (Figure 6). At our sites, the $\varepsilon_{C29/C23}$ distributions reveal that the δ^2H of alkane C_{29} preserved in sediments averaged ~22 ‰ lower than those of alkane C_{23} (Figure 6, dark gray box plot). Comparisons with $\varepsilon_{C29/C23}$ based on alkanes from different plant sources highlight similarities in the isotopic composition of sediments and terrestrial plants. The differences in δ^2H between alkanes C_{29} and C_{23} in angiosperms and gymnosperms are within 4 ‰ of the $\varepsilon_{C29/C23}$ of the sediments (Figure 6, dark and light green box plots). Grasses differ, however, with the $\varepsilon_{C29/C23}$ based on grass alkanes ~16 ‰ larger on average than in sediments (grass mean $\varepsilon_{C29/C23}$ =-38 ‰). Submerged aquatic plants, often assumed to be a major source of C_{23}, represent a more extreme difference still with a positive $\varepsilon_{C29/C23}$. On average, the δ^2H of alkane C_{29} of submerged aquatic plants is ~10 ‰ higher than for C_{23} (Figure 6, blue box plot).

Assuming a constant angiosperm source for the C_{29} alkanes in sediments, but different plant sources of alkane C_{23}, produces a range of different outcomes (Figure 6, light gray box plots on right). Gymnosperm tree or grass sources of alkane C_{23} resulted in higher $\varepsilon_{C29/C23}$ values (means of -13 ‰ and -3.4 ‰, respectively) than those observed in sediments. Moreover, submergent aquatic plant sources of alkane C_{23} produced positive $\varepsilon_{C29/C23}$ values suggesting that the δ^2H of C_{29} alkane in angiosperms is consistently more positive (by ~56 ‰) than the δ^2H of C_{23} alkane in aquatic plants. Such mixed source $\varepsilon_{C29/C23}$ distributions are inconsistent with most of the C_{29}/C_{23} differences in our sediment samples and affirm that most sedimentary alkanes come from consistent terrestrial plant sources.

3.6 Comparison with global sedimentary wax δ^2H

The δ^2H from water and alkanes (for both C_{23} and C_{29}) plot consistently (Figure 7, red points) along with other global δ^2H datasets (grey and blue points) compiled by McFarlin et al. (2019) with additional data from Ladd et al. (2021). Our 30 new measurements of δ^2H in C_{29} alkane from surface sediments do not depart from the global relationship with the δ^2H of MAP (Figure 7A). Adding our data, updates the global relationship to

$$C_{29}\ \delta^2H\ ‰ = 0.76 \times (\text{MAP}\ \delta^2H\ ‰) - 132,$$

and slightly improves the coefficient of determination (r^2) from 0.83 to 0.84; McFarlin et al., (2019) found that

$$C_{29}\ \delta^2H\ ‰ = 0.78 \times (\text{MAP}\ \delta^2H\ ‰) - 129.$$

We also find that, at a global scale, alkane C_{29} δ^2H measurements from sediments are significantly correlated to lake water δ^2H (r^2=0.64, $p<0.001$) (Figure 7B). Although there is more scatter in the relationship between the δ^2H of C_{29} and lake water than with MAP, the scatter

clusters around sites from high latitudes (>65°N) where lake water δ^2H can be decoupled from MAP (Culet and Thomas, 2020; Thomas et al., 2020).

In the case of the C_{23} alkane (Figure 7, lower panel), our additional δ^2H measurements also improve the global relationships with both MAP and lake water δ^2H (r^2= 0.52 and 0.63, respectively, compared to r^2= 0.3 and 0.4, respectively, from McFarlin et al., 2019). Importantly, however, the slopes of the updated global relationships for MAP and lake water do not differ, within uncertainty error, from each other or from the C_{29} relationship above: 0.76 (s.e.= 0.08) for MAP and 0.73 (s.e. = 0.07) for lake water (Figure 7C,D).

Consequently, we find no significant differences in the predicted δ^2H of MAP or lake water (Figure 8A) based on the linear relationships for sediment C_{29} and C_{23}, respectively (Figure 7A,C). The overlap between predicted MAP δ^2H and predicted lake water δ^2H is consistent with the similar correlations of δ^2H among MAP, lake water, and both C_{29} and C_{23} (Figure 7). In parallel, we find no correlation between the C_{29}-C_{23} δ^2H difference ($\varepsilon_{C29/C23}$) in sediments and the MAP-lake water δ^2H difference ($\varepsilon_{MAP/LW}$) related to evaporation (Figure 8B). Instead, we detect a significant correlation between C_{23} δ^2H and C_{29} δ^2H (Figure 8C-E) suggesting common sources of sedimentary C_{23} and C_{29} alkanes.

The δ^2H of C_{25} and C_{27} also correlate significantly with C_{29} δ^2H suggesting that both mid- and long-chain alkanes in sediments are likely derived from higher terrestrial plants (Figure 8D-E). The scatter in the relationship between C_{23} and C_{29} (Figure 8E) could suggest a mix of C_{23} sources (e.g., aquatic vs. terrestrial), but the statistically significant relationship (Pearson's r = 0.80) between the δ^2H values of the two alkanes suggests a dominant terrestrial source. Furthermore, the intercepts of the global correlations (Figure 8C-E) agree with the ε_{app} distributions found by comparing sediments and angiosperm trees (Figure 5).

Some of the data might represent aquatically-derived C_{23} (i.e., samples with high $\varepsilon_{C29/C23}$ values overlapping with the $\varepsilon_{C29/C23}$ range expected by mixing submerged and terrestrial sources, gray box plot, Figure 8B), but the global dataset supports a dominantly terrestrial source of sedimentary C_{23}. Most $\varepsilon_{C29/C23}$ values in the global sediment dataset (89 %) lie below the $\varepsilon_{angiospermC29/submergedC23}$ mean (gray box plot, Figure 8B), and 84 % fall within the $\varepsilon_{angiospermC29/angiospermC23}$ distribution (dark green box plot, Figure 8B). Some points may, however, represent grass-derived alkanes (light green box plot, Figure 8B).

4. Discussion

4.1. Provenance of mid- and long-chain n-alkanes in sedimentary archives

Both mid- and long-chain n-alkanes in lake sediments from mid-latitude North America likely derive from higher terrestrial plants. The n-alkane distribution in sediments is most similar to that in terrestrial plants where n-alkane abundances increase with increasing chain-length (Figure 3). Consistent with previous findings (Ficken et al., 2000; Gao et al., 2011), the n-alkane distributions in aquatic floating and emergent plants also show a similar pattern to terrestrial plants with abundant long-chain n-alkanes. Conversely, and also consistent with previous studies, the n-alkane distributions in aquatic algae favor the short-chain alkane C_{17} (Sachse et al., 2004), while the n-alkane distributions in aquatic submerged plants maximize on the mid-chain alkane C_{23} (Ficken et al., 2000; Gao et al., 2011). However, terrestrial plants also synthesize mid-chain n-alkanes, even if their relative abundance compared to long-chain n-alkanes is lower than in submerged aquatic sources (Figure 3). Consequently, sedimentary C_{23} might appear derived from aquatic submerged plants, but the δ^2H values of n-alkanes do not support such an inference. The δ^2H in plants and sediments suggest a terrestrial source of mid-chain n-alkanes in sediments (Figure 5-6).

346 The distributions of apparent fractionation factors support a dominantly angiosperm tree
347 source of mid- and long-chain n-alkanes in sediments where the average $\varepsilon_{wax/MAP}$ values for
348 angiosperm trees fall within 4 ‰ for alkane C_{23} and within 1 ‰ for alkane C_{29} of those for
349 sediments (t-test $p>0.05$, Figure 5). Moreover, the mean $\varepsilon_{C23/MAP}$ and $\varepsilon_{C29/MAP}$ for grasses and
350 aquatic plants are significantly lower (by >15 ‰; t-test $p<0.05$) than those of sediments. While
351 the mean $\varepsilon_{C23/MAP}$ and $\varepsilon_{C29/MAP}$ for algae are not significantly different than those of sediments,
352 more than 75% of their distributions plot below the sediment means (Figure 5). Furthermore, the
353 difference in the ε_{app} distributions between sediments and aquatic plants is slightly larger if we
354 consider the ε_{app} between n-alkanes and lake water for sediments and aquatic plants (Table 3).
355 The lower ε_{app} values in submergent aquatic plants compared to angiosperms and gymnosperms
356 is consistent with previous findings (Chikaraishi and Naraoka, 2003; Duan et al., 2014; Aichner
357 et al., 2017).

358 Our result challenges the assumption that submerged aquatic plants produce the C_{23}
359 incorporated in sediments, which has led to the use of $\varepsilon_{C29/C23}$ as a proxy for terrestrial
360 evapotranspiration (i.e., $\varepsilon_{terr\text{-}aquatic}$; Seki et al., 2011; Rach et al., 2014, Rach et al., 2017; Curtin et
361 al., 2019). The rationale behind this assumption is that long-chain n-alkanes in terrestrial plants
362 (e.g., C_{29}) track the δ^2H of MAP composition plus an additional enrichment from soil and leaf
363 water evaporation (Sachse et al., 2004). If lake water can be assumed to have experienced little
364 evaporative enrichment, then the C_{23} alkanes in submergent aquatic plants should track the
365 original δ^2H of the MAP; if not, C_{23} could record the δ^2H signature of amplified evaporation
366 within a lake. Either way, the $\varepsilon_{C29/C23}$ values would reflect the strength of either soil or lake
367 evaporation depending upon the sign of the difference. Such a range of outcomes could be

368 supported given that the mean ε_{app} between the δ^2H values of C_{29} and those of C_{23} in sediments is
369 -22 ‰ with a large standard deviation of 24‰ (Figure 6).

370 However, the apparent fractionation factor varies between individual n-alkanes and
371 within individual groups (Figure 5) and $\varepsilon_{C29/C23}$ values in sediments are similar those observed
372 within individual plant groups such as in angiosperm and gymnosperm trees (Figure 6).
373 Moreover, if submerged aquatic plants would be the dominant source of C_{23} and higher
374 terrestrial plants the dominant source of C_{29} (e.g., angiosperms) in sediments at our sites, then the
375 mean values of $\varepsilon_{C29/C23}$ in sediments would be positive (mean $\varepsilon_{angiospermC29/submergedC23}$= 34 ‰;
376 Figure 6). Instead, the observed offsets in most sediments appear because C_{23} δ^2H values are
377 systematically more positive than C_{29} δ^2H values by ~23 ‰ in higher terrestrial plants (Fig 5).
378 Consequently, $\varepsilon_{C29/C23}$ signifies variations in ε_{app} between the C_{23} and C_{29} alkanes, which
379 typically should not be interpreted as changes in evaporation.

380 The dominance of terrestrial angiosperm trees as the source of mid- and long-chain
381 alkanes in the lake sediments could be explained by differences in: (1) aquatic versus terrestrial
382 tree distributions in and around lakes, and (2) the rate of n-alkane production in aquatic versus
383 terrestrial plants (Dion-Kirschner et al., 2020). In general, the distribution of submerged aquatic
384 plants is limited to the aquatic near-shore zone of lakes where photosynthesis can occur (Jiang et
385 al., 2021). Conversely, terrestrial plants extend over large water- and air-sheds around most
386 lakes. In addition, previous studies have shown that aquatic plants produce 30x less leaf-waxes
387 while shoreline plants produce 10-300x less leaf-waxes than terrestrial plants per unit of leaf
388 biomass (µg/g; Freimuth et al., 2019; Dion-Kirschner et al., 2020). Consequently, both greater
389 rates of alkane production on terrestrial tree leaves and the greater extent of terrestrial
390 ecosystems combine to favor angiosperm tree leaf-wax contribution to the sediments, masking

391 the weak signal of mid-chain n-alkanes produced by aquatic plants. Even though terrestrial plants
392 synthesize less mid-chain than long-chain n-alkanes (Figure 3), terrestrial trees act as the
393 dominant sources for both chain lengths (Diefendorf and Freimuth, 2017). Therefore, we
394 recommend the use of other lake water isotopic proxies such as short-chain alkanes and alkanoic
395 acids that are primarily synthesized by algae (Sachse et al., 2012).

396 **4.2 ε_{app} as a function of vegetation type**

397 In our dataset, ε_{app} varies within and between individual plant groups and, therefore,
398 individual plant groups have different influences on the ε_{app} values of n-alkanes deposited in
399 sedimentary archives (Figure 5, Table 3). Thus, information on the vegetation contributing to the
400 sedimentary alkane pool is crucial for inferring the δ^2H of the source water. Below we discuss
401 the impact of vegetation changes on alkane C_{29}, as C_{29} is the most abundant alkane in sediments
402 and most commonly used for inferring the δ^2H of precipitation.

403 Consistent with previous findings (Chikaraishi and Naraoka, 2003), we find that $\varepsilon_{C29/MAP}$
404 values in angiosperm trees are similar to those in gymnosperm trees (means within 6 ‰; Figure
405 5, Table 3) suggesting that vegetation shifts between angiosperms and gymnosperms trees would
406 not impact C_{29} δ^2H signatures in sedimentary archives. The similar $\varepsilon_{C29/MAP}$ (within 4 ‰) at our
407 two most extremely different angiosperm and gymnosperm sites (Figure 4) demonstrate that the
408 δ^2H of sedimentary C_{29} alkane should track the δ^2H of source water with a relatively constant ε_{app}
409 even if shifts in vegetation sources do occur (i.e., angiosperm trees to gymnosperm trees, or vice
410 versa). Therefore, associated changes in C_{29} δ^2H can be interpreted as changes in water source
411 δ^2H. Nevertheless, while $\varepsilon_{C29/MAP}$ in angiosperm and gymnosperm trees does appear to be similar
412 at our sites, the decomposed seasonal precipitation signal and $\varepsilon_{C29/MAP}$ values might indeed be
413 different at other sites.

414 Grasses may present a challenge, however. The $\varepsilon_{C29/MAP}$ distribution of grasses deviate
415 from either angiosperm or gymnosperm trees, and a change from either source to grasses (or vice
416 versa) would produce a significant shift in the δ^2H of sedimentary C_{29}. Our data support previous
417 findings (Sachse et al., 2012; Bush and McInerney et al., 2013; Wang et al., 2018) and show that
418 the mean $\varepsilon_{C29/MAP}$ in grasses (-162 ‰) is ~29 ‰ lower than in angiosperm and gymnosperm
419 trees, respectively (Figure 5). A shift favoring grass inputs to the sediments would decrease C_{29}
420 δ^2H by ~29 ‰. Therefore, constraints on grass inputs should be evaluated. Previous efforts to
421 distinguish between trees and grass inputs using the ratio of the abundance of alkanes C_{31} and
422 C_{29} have been unsuccessful because this ratio is highly variable in both grasses and higher
423 terrestrial plants (Bush and McInerney, 2013). Other methods using $\delta^{13}C$ successfully distinguish
424 between C4 and C3 plants (Tiereny et al., 2017; Bhattacharya et al., 2018). However, this tool
425 does not apply well to temperate grasslands dominated by C3 plants. Instead, the differences in
426 $\varepsilon_{C29/C23}$ values between different plant groups may provide information on the dominant
427 vegetation (Figure 6). The mean $\varepsilon_{C29/C23}$ in angiosperms (-18 ‰) is statistically different than the
428 mean for grasses (-38‰; Student's t test; $p=0.006$), although the grass and gymnosperm means
429 do not differ significantly (Student's t test; $p>0.05$). Consequently, $\varepsilon_{C29/C23}$ values below -38 ‰
430 (i.e., the mean $\varepsilon_{C29/C23}$ in grasses) can potentially imply that grasses dominate the alkane C_{29}
431 inputs to sedimentary archives, especially when accompanied with a 29 ‰ decline in C_{29} δ^2H.

432 Submerged aquatic plants may also represent an important lipid source that would affect
433 the δ^2H of both C_{29} and C_{23} in sediments (Figure 5-6). Our data suggest that $\varepsilon_{alkane/MAP}$ values are
434 ~17 ‰ and ~43 ‰ more negative in submerged aquatic plants than in angiosperms in C_{29} and
435 C_{23} alkanes, respectively (Figure 5). As with grasses, $\varepsilon_{C29/C23}$ may also help to distinguish
436 between submerged aquatic plant and angiosperm inputs (Figure 6). Submerged aquatic plants

have a $\varepsilon_{C29/C23}$ distribution with a mean of 10 ‰, which differs from that in angiosperm trees, gymnosperm trees, or grasses (Figure 6). While C_{23} δ^2H is more positive than C_{29} δ^2H in angiosperm tree, gymnosperm trees, and grasses, it is more negative in submerged aquatic plants. However, a dominant submerged aquatic source of C_{29} alkane is unlikely (Figure 2), except in the absence of higher terrestrial plants around the lakes as is the case with desert lakes (Wang et al., 2018).

Submerged aquatic plants may, conversely, represent an important source of C_{23} alkane (Ficken et al., 2000, Puleo et al., 2020), but that does not appear to be the case at most of our sites. Higher terrestrial plants generate most of the C_{23} alkane based on isotopic compositions (Figure 5) and $\varepsilon_{C29/C23}$ distributions (Figure 6). If the sedimentary C_{23} source is aquatic submergent plants, the $\varepsilon_{C29angiosperm/C23submerged}$ distribution should be ~52 ‰ more positive than sediments with a higher terrestrial plant source (mean $\varepsilon_{C29angiosperm/C23submerged}$ = 34‰). Consequently, $\varepsilon_{C29/C23}$ values in sediments equal or greater than the mean of $\varepsilon_{C29angiosperm/C23submerged}$ from our study sites (34 ‰) are indicative of aquatic submerged plant input and, therefore, the δ^2H signature of C_{23} can be used as a proxy for lake-water δ^2H in those cases.

4.3 Global relationship between mid- and long chain n-alkanes to environmental waters

Previous studies show that the δ^2H of alkane C_{29} and MAP correlate well at a global scale (Sachse et al., 2012; McFarlin et al., 2019; Ladd et al., 2021), and our results do not depart from this relationship (Figure 7A). However, while our δ^2H measurements improve the relationships between alkanes C_{23} and C_{29} to environmental waters (McFarlin et al., 2019), they indicate that the δ^2H of alkane C_{23} is likely also linked to that of MAP rather than lake water δ^2H signatures (Figure 8). Several possible factors might influence these relationships.

First, higher terrestrial plant input to sedimentary archives at a global scale must generally dominate the alkane C_{23} pool (Sachse et al., Liu and Liu, 2019). The δ^2H of n-alkane from higher terrestrial plants at our sites show similar $\varepsilon_{C23/MAP}$ distributions to those detected in sediments, which is more positive than detected for aquatic sources (Figure 5). Second, lake water δ^2H during the spring closely tracks the δ^2H of MAP with an average $\varepsilon_{Lake/MAP}$ of 10 ± 16 ‰ (Figure 2). Likewise, the global $\varepsilon_{Lake/MAP}$ distribution has a mean of 9 ± 25 ‰ (Figure 8B). Consequently, the relationships between the δ^2H of individual n-alkanes and those of MAP or lake water are driven by the apparent fractionation factor (ε_{app}) while differences between those relationships can be explained by $\varepsilon_{Lake/MAP}$ (Figure 7). Therefore, the updated global dataset confirms that: (1) both C_{23} and C_{29} alkanes are likely derived from higher terrestrial plants, and (2) the global relationships between the δ^2H values of n-alkanes and environmental waters are determined by both ε_{app} and $\varepsilon_{Lake/MAP}$. We speculate that the scatter in the relationship between observed versus predicted lake water δ^2H values is the result of a dominant higher terrestrial plant input to sedimentary archives, which generates a poor relationship between C_{23} and lake water δ^2H values at sites where MAP and lake water δ^2H values are decoupled (Cluett and Thomas, 2020; Thomas et al., 2020).

At our sites, modeled MAP and measured lake water δ^2H and $\delta^{18}O$ are strongly correlated and plot near the GMWL (Figure 2). While some of the lake water δ^2H measurements deviate from the GMWL (Figure 2A), suggesting varying degrees of evaporative enrichment, the average $\varepsilon_{Lake/MAP}$ value of 10 ‰ suggests that lake water δ^2H values during the spring are on average 10 ‰ more positive than modeled MAP. We further show that both measured lake water and modeled MAP δ^2H values significantly correlate with modeled seasonal precipitation δ^2H values (Table 2) but have the strongest relationships to modeled spring δ^2H values (Pearson's

r=0.88 and 0.97, respectively). A strong correlation between measured lake water and modeled spring precipitation δ^2H values is expected because lake water at our sites were sampled during the spring season. However, the strong correlation (Pearson's r=0.97) between MAP and spring season precipitation δ^2H values suggests that MAP δ^2H values at our sites are mainly controlled by spring precipitation δ^2H. Therefore, because MAP δ^2H has the strongest correlation to spring precipitation δ^2H and because lake water δ^2H shows the strongest correlation to MAP δ^2H (Pearson's r=0.92), both lake water and MAP δ^2H values at our sites carry a spring precipitation signal. Since leaf-wax n-alkanes have been shown to track the δ^2H signatures of source moisture during leaf-formation (Tipple et al., 2013), which is spring season at our sites, leaf-wax n-alkanes in plants and sediments should track modeled MAP δ^2H composition at our sites.

Even though most of the lakes from the global dataset closely track the δ^2H signatures of precipitation, some sites show a clear decoupling between lake water and MAP (i.e., extremely low or high $\varepsilon_{Lake/MAP}$ values Figure 8B). Furthermore, the global $\varepsilon_{C29/C23}$ distribution supports the hypothesis that on a global scale, the dominant source for alkane C_{23} in sedimentary archives is of higher terrestrial plant origin (Figure 8B). A dominant terrestrial source of mid- and long-chain n-alkanes to sedimentary archives is also supported by the strong correlations between the C_{29} alkane and other mid-and long-chain n-alkanes (Figure 8C-D).

Given large uncertainties in $\varepsilon_{alkane/water}$ values within and between individual plant groups (Figure 5, Table 3; also see Sachse et al., 2012 and Liu and Liu 2016) and the strong correlation between MAP and lake water δ^2H values at our sites (Figure 2) and at a global scale (Figure 8b), even if the dominant source for the C_{23} alkane to sedimentary archives would be of aquatic origin, absolute differences between MAP and lake water δ^2H values would be difficult to constrain. Therefore, given large uncertainties in ε_{app}, we strongly caution against

evapotranspiration inferences even at sites where lake water δ^2H signatures can be constrained with the use of aquatically derived C_{23} alkane.

5. Conclusions

Comparisons of the relative abundances and δ^2H of n-alkanes in plants and sediments from across mid-latitude North America demonstrate that both mid- and long-chain n-alkanes (i.e., C_{23} and C_{29}) in lake sediments commonly derive from higher terrestrial plants. Most likely, the dominant terrestrial leaf-wax input to sedimentary archives is driven by terrestrial vegetation because terrestrial plants cover larger source areas and have higher rates of leaf-wax production compared to aquatic plants. We show that ε_{app} varies as a function of n-alkane chain length and individual plant groups, and that at our sites, ε_{app} values in surface sediments parallel those observed in higher terrestrial plants (i.e., angiosperm trees and gymnosperm trees) rather than those in grasses or in aquatic plants. Our data, therefore, are inconsistent with the assumption that the δ^2H of mid-chain n-alkanes can be used as proxy for lake water isotopic composition or that the offset between C_{23} and C_{29} δ^2H can be used as a proxy for evaporation ($\varepsilon_{C29/C23}$).

The similarities between ε_{app} in sediments, angiosperm and gymnosperm trees indicate a dominant higher-terrestrial plant leaf-wax input to sedimentary archives, but also show that vegetation shifts between angiosperm and gymnosperm trees would not have an impact on ε_{app} values. Therefore, changes in leaf-wax δ^2H composition preserved in sedimentary archives can be interpreted as changes in the δ^2H of source water, especially during vegetation shifts between angiosperm and gymnosperms tree communities. Grasses produce a significant exception, however, because the δ^2H of C_{29} in grasses are on average 32 ‰ lower than in angiosperms and 26 ‰ lower than in gymnosperms.

Acknowledgments

We thank James G. Sanford, David T. Liefert and Laurie Grigg for field work assistance. This work was supported by the Roy J. Shlemon Center for Quaternary Studies at the University of Wyoming, by the Department of Geology and Geophysics at the University of Wyoming, and by the Microbial Ecology Collaborative Project at the University of Wyoming through the National Science Foundation grant EPS-1655726.

Research Data associated with this article can be accessed at https://doi.org/10.15786/20126483.

References

Aichner, B., Herzschuh, U. and Wilkes, H., (2010b). Influence of aquatic macrophytes on the stable carbon isotopic signatures of sedimentary organic matter in lakes on the Tibetan Plateau. Organic Geochemistry, 41(7), pp.706-718.

Aichner, B., Herzschuh, U., Wilkes, H., Vieth, A. and Böhner, J., (2010a). δD values of n-alkanes in Tibetan lake sediments and aquatic macrophytes–A surface sediment study and application to a 16 ka record from Lake Koucha. Organic Geochemistry, 41(8), pp.779-790.

Aichner, B., Hilt, S., Périllon, C., Gillefalk, M. and Sachse, D., (2017). Biosynthetic hydrogen isotopic fractionation factors during lipid synthesis in submerged aquatic macrophytes: Effect of groundwater discharge and salinity. Organic Geochemistry, 113, pp.10-16.

Bhattacharya, T., Tierney, J.E., Addison, J.A. and Murray, J.W., (2018). Ice-sheet modulation of deglacial North American monsoon intensification. Nature Geoscience, 11(11), pp.848-852.

Bowen, G. J. (2020): Gridded maps of the isotopic composition of meteoric waters. http://www.waterisotopes.org

Bush, R.T. and McInerney, F.A., (2013). Leaf wax n-alkane distributions in and across modern plants: implications for paleoecology and chemotaxonomy. Geochimica et Cosmochimica Acta, 117, pp.161-179.

Chikaraishi, Y. and Naraoka, H., (2003). Compound-specific δD–δ13C analyses of n-alkanes extracted from terrestrial and aquatic plants. Phytochemistry, 63(3), pp.361-371.

Cluett, A.A. and Thomas, E.K., (2020). Resolving combined influences of inflow and evaporation on western Greenland lake water isotopes to inform paleoclimate inferences. Journal of Paleolimnology, pp.1-18.

Craig, H. (1961). Isotopic variations in meteoric waters. Science, 133(3465), 1702-1703.

Criss, R. E. (1999). Principles of stable isotope distribution. Oxford University Press on Demand.

Curtin, L., D'Andrea, W.J., Balascio, N., Pugsley, G., de Wet, G. and Bradley, R., (2019). Holocene and Last Interglacial climate of the Faroe Islands from sedimentary plant wax hydrogen and carbon isotopes. Quaternary Science Reviews, 223, p.105930.

Daniels, W.C., Russell, J.M., Giblin, A.E., Welker, J.M., Klein, E.S. and Huang, Y., (2017). Hydrogen isotope fractionation in leaf waxes in the Alaskan Arctic tundra. Geochimica et Cosmochimica Acta, 213, pp.216-236.

Diefendorf, A.F., Freeman, K.H., Wing, S.L. and Graham, H.V., (2011). Production of n-alkyl lipids in living plants and implications for the geologic past. Geochimica et Cosmochimica Acta, 75(23), pp.7472-7485.

572 Diefendorf, A.F., Sberna, D.T. and Taylor, D.W., (2015). Effect of thermal maturation on plant-
573 derived terpenoids and leaf wax n-alkyl components. Organic Geochemistry, 89, pp.61-
574 70.
575 Diefendorf, A.F. and Freimuth, E.J., (2017). Extracting the most from terrestrial plant-derived n-
576 alkyl lipids and their carbon isotopes from the sedimentary record: A review. Organic
577 Geochemistry, 103, pp.1-21.
578 Dion-Kirschner, H., McFarlin, J.M., Masterson, A.L., Axford, Y. and Osburn, M.R., (2020).
579 Modern constraints on the sources and climate signals recorded by sedimentary plant
580 waxes in west Greenland. Geochimica et Cosmochimica Acta, 286, pp.336-354.
581 Douglas, P.M., Pagani, M., Brenner, M., Hodell, D.A. and Curtis, J.H., (2012). Aridity and
582 vegetation composition are important determinants of leaf-wax δD values in southeastern
583 Mexico and Central America. Geochimica et Cosmochimica Acta, 97, pp.24-45.
584 Duan, Y., Wu, B., Xu, L., He, J. and Sun, T., (2011). Characterization of n-alkanes and their
585 hydrogen isotopic composition in sediments from Lake Qinghai, China. Organic
586 geochemistry, 42(7), pp.720-726.
587 Duan, Y., Wu, Y., Cao, X., Zhao, Y. and Ma, L., (2014). Hydrogen isotope ratios of individual
588 n-alkanes in plants from Gannan Gahai Lake (China) and surrounding area. Organic
589 geochemistry, 77, pp.96-105.
590 Feakins, S.J., Peters, T., Wu, M.S., Shenkin, A., Salinas, N., Girardin, C.A., Bentley, L.P.,
591 Blonder, B., Enquist, B.J., Martin, R.E. and Asner, G.P., (2016). Production of leaf wax
592 n-alkanes across a tropical forest elevation transect. Organic Geochemistry, 100, pp.89-
593 100.

Feakins, S.J., Wu, M.S., Ponton, C., Galy, V. and West, A.J., (2018). Dual isotope evidence for sedimentary integration of plant wax biomarkers across an Andes-Amazon elevation transect. Geochimica et Cosmochimica Acta, 242, pp.64-81.

Ficken, K.J., Li, B., Swain, D.L. and Eglinton, G., (2000). An n-alkane proxy for the sedimentary input of submerged/floating freshwater aquatic macrophytes. Organic geochemistry, 31(7-8), pp.745-749.

Freimuth, E.J., Diefendorf, A.F., Lowell, T.V., Bates, B.R., Schartman, A., Bird, B.W., Landis, J.D. and Stewart, A.K., (2020). Contrasting sensitivity of lake sediment n-alkanoic acids and n-alkanes to basin-scale vegetation and regional-scale precipitation δ2H in the Adirondack Mountains, NY (USA). Geochimica et Cosmochimica Acta, 268, pp.22-41.

Freimuth, E.J., Diefendorf, A.F., Lowell, T.V. and Wiles, G.C., (2019). Sedimentary n-alkanes and n-alkanoic acids in a temperate bog are biased toward woody plants. Organic Geochemistry, 128, pp.94-107.

Gao, L., Hou, J., Toney, J., MacDonald, D. and Huang, Y., (2011). Mathematical modeling of the aquatic macrophyte inputs of mid-chain n-alkyl lipids to lake sediments: Implications for interpreting compound specific hydrogen isotopic records. Geochimica et Cosmochimica Acta, 75(13), pp.3781-3791.

Garcin, Y., Schwab, V.F., Gleixner, G., Kahmen, A., Todou, G., Séné, O., Onana, J.M., Achoundong, G. and Sachse, D., (2012). Hydrogen isotope ratios of lacustrine sedimentary n-alkanes as proxies of tropical African hydrology: insights from a calibration transect across Cameroon. Geochimica et Cosmochimica Acta, 79, pp.106-126.

Guenther, F., Aichner, B., Siegwolf, R., Xu, B., Yao, T. and Gleixner, G., (2013). A synthesis of hydrogen isotope variability and its hydrological significance at the Qinghai–Tibetan Plateau. Quaternary International, 313, pp.3-16.

He, D., Ladd, S.N., Saunders, C.J., Mead, R.N. and Jaffé, R., (2020). Distribution of n-alkanes and their δ2H and δ13C values in typical plants along a terrestrial-coastal-oceanic gradient. Geochimica et Cosmochimica Acta, 281, pp.31-52.

Jetter, R., Kunst, L., Samuels, A.L., Riederer, M. and Müller, C., (2006). Biology of the plant cuticle. Composition of plant cuticular waxes, pp.145-181.

Jiang, J., Meng, B., Liu, H., Wang, H., Kolpakova, M., Krivonogov, S., Song, M., Zhou, A., Liu, W. and Liu, Z., (2021). Water depth control on n-alkane distribution and organic carbon isotope in mid-latitude Asian lakes. Chemical Geology, 565, p.120070.

Ladd, S.N., Maloney, A.E., Nelson, D.B., Prebble, M., Camperio, G., Sear, D.A., Hassall, J.D., Langdon, P.G., Sachs, J.P. and Dubois, N., (2021). Leaf wax hydrogen isotopes as a hydroclimate proxy in the tropical Pacific. Journal of Geophysical Research: Biogeosciences, 126(3), p.e2020JG005891.

Leider, A., Hinrichs, K.U., Schefuß, E. and Versteegh, G.J., (2013). Distribution and stable isotopes of plant wax derived n-alkanes in lacustrine, fluvial and marine surface sediments along an Eastern Italian transect and their potential to reconstruct the hydrological cycle. Geochimica et Cosmochimica Acta, 117, pp.16-32.

Liefert, D.T., Shuman, B.N., Parsekian, A.D. and Mercer, J.J., (2018). Why are some rocky mountain lakes ephemeral?. Water Resources Research, 54(8), pp.5245-5263.

637 Liu, H. and Liu, W., (2016). n-Alkane distributions and concentrations in algae, submerged
638 plants and terrestrial plants from the Qinghai-Tibetan Plateau. Organic geochemistry, 99,
639 pp.10-22.
640 Liu, H. and Liu, W., (2019). Hydrogen isotope fractionation variations of n-alkanes and fatty
641 acids in algae and submerged plants from Tibetan Plateau lakes: Implications for
642 palaeoclimatic reconstruction. Science of the Total Environment, 695, p.133925.
643 Liu, X., Feakins, S.J., Dong, X., Xue, Q., Marek, T., Leskovar, D.I., Neely, C.B. and Ibrahim,
644 A.M., (2017). Experimental study of leaf wax n-alkane response in winter wheat cultivars
645 to drought conditions. Organic Geochemistry, 113, pp.210-223.
646 Mead, R., Xu, Y., Chong, J. and Jaffé, R., (2005). Sediment and soil organic matter source
647 assessment as revealed by the molecular distribution and carbon isotopic composition of
648 n-alkanes. Organic Geochemistry, 36(3), pp.363-370.
649 McFarlin, J.M., Axford, Y., Masterson, A.L. and Osburn, M.R., (2019). Calibration of modern
650 sedimentary δ2H plant wax-water relationships in Greenland lakes. Quaternary Science
651 Reviews, 225, p.105978.
652 Mügler, I., Sachse, D., Werner, M., Xu, B., Wu, G., Yao, T. and Gleixner, G., (2008). Effect of
653 lake evaporation on δD values of lacustrine n-alkanes: A comparison of Nam Co (Tibetan
654 Plateau) and Holzmaar (Germany). Organic Geochemistry, 39(6), pp.711-729.
655 Nelson, D.B., Ladd, S.N., Schubert, C.J. and Kahmen, A., (2018). Rapid atmospheric transport
656 and large-scale deposition of recently synthesized plant waxes. Geochimica et
657 Cosmochimica Acta, 222, pp.599-617.

Pagani, M., Pedentchouk, N., Huber, M., Sluijs, A., Schouten, S., Brinkhuis, H., Damsté, J.S.S. and Dickens, G.R., (2006). Arctic hydrology during global warming at the Palaeocene/Eocene thermal maximum. Nature, 442(7103), pp.671-675.

Peaple, M.D., Tierney, J.E., McGee, D., Lowenstein, T.K., Bhattacharya, T. and Feakins, S.J., (2021). Identifying plant wax inputs in lake sediments using machine learning. Organic Geochemistry, 156, p.104222.

Polissar, P.J. and Freeman, K.H., (2010). Effects of aridity and vegetation on plant-wax δD in modern lake sediments. Geochimica et Cosmochimica Acta, 74(20), pp.5785-5797.

PRISM Climate Group, Oregon State University, http://prism.oregonstate.edu, created June 2019.

Puleo, P.J., Axford, Y., McFarlin, J.M., Curry, B.B., Barklage, M. and Osburn, M.R., (2020). Late glacial and Holocene paleoenvironments in the midcontinent United States, inferred from Geneva Lake leaf wax, ostracode valve, and bulk sediment chemistry. *Quaternary Science Reviews*, *241*, p.106384.

R Core Team (2018). R: A language and environment for statistical computing. R Foundation for Statistical Computing, Vienna, Austria. URL https://www.R-project.org/.

Rach, O., Brauer, A., Wilkes, H. and Sachse, D., (2014). Delayed hydrological response to Greenland cooling at the onset of the Younger Dryas in western Europe. Nature Geoscience, 7(2), pp.109-112.

Rach, O., Kahmen, A., Brauer, A. and Sachse, D., (2017). A dual-biomarker approach for quantification of changes in relative humidity from sedimentary lipid D/H ratios. Climate of the Past, 13(7), pp.741-757.

Regan, C. M., R. C. Musselman, and J. D. Haines, (1998). Vegetation of the Glacier Lakes Ecosystem Experiments Site. USDA Forest Service - Rocky Mountain Research Station Research Paper.

Sachse, D., Radke, J. and Gleixner, G., (2004). Hydrogen isotope ratios of recent lacustrine sedimentary n-alkanes record modern climate variability. *Geochimica et Cosmochimica Acta*, *68*(23), pp.4877-4889.

Sachse, D., Gleixner, G., Wilkes, H. and Kahmen, A., (2010). Leaf wax n-alkane δD values of field-grown barley reflect leaf water δD values at the time of leaf formation. *Geochimica et Cosmochimica Acta*, *74*(23), pp.6741-6750.

Sachse, D., Billault, I., Bowen, G.J., Chikaraishi, Y., Dawson, T.E., Feakins, S.J., Freeman, K.H., Magill, C.R., McInerney, F.A., Van Der Meer, M.T. and Polissar, P., (2012). Molecular paleohydrology: interpreting the hydrogen-isotopic composition of lipid biomarkers from photosynthesizing organisms. Annual Review of Earth and Planetary Sciences, 40, pp.221-249.

Schefuß, E., Schouten, S. and Schneider, R.R., (2005). Climatic controls on central African hydrology during the past 20,000 years. *Nature*, *437*(7061), pp.1003-1006.

Schimmelmann, A., Sessions, A.L. and Mastalerz, M., (2006). Hydrogen isotopic (D/H) composition of organic matter during diagenesis and thermal maturation. *Annu. Rev. Earth Planet. Sci.*, *34*, pp.501-533.

Seki, O., Nakatsuka, T., Shibata, H. and Kawamura, K., (2010). A compound-specific n-alkane δ13C and δD approach for assessing source and delivery processes of terrestrial organic matter within a forested watershed in northern Japan. *Geochimica et Cosmochimica Acta*, *74*(2), pp.599-613.

703 Seki, O., Meyers, P.A., Yamamoto, S., Kawamura, K., Nakatsuka, T., Zhou, W. and Zheng, Y.,
704 (2011). Plant-wax hydrogen isotopic evidence for postglacial variations in delivery of
705 precipitation in the monsoon domain of China. Geology, 39(9), pp.875-878.
706 Sessions, A.L., Sylva, S.P., Summons, R.E. and Hayes, J.M., (2004). Isotopic exchange of
707 carbon-bound hydrogen over geologic timescales. *Geochimica et Cosmochimica*
708 *Acta*, *68*(7), pp.1545-1559.
709 Sessions, A.L., (2016). Factors controlling the deuterium contents of sedimentary
710 hydrocarbons. *Organic Geochemistry*, *96*, pp.43-64.
711 Thomas, E.K., Hollister, K.V., Cluett, A.A. and Corcoran, M.C., (2020). Reconstructing Arctic
712 precipitation seasonality using aquatic leaf wax δ2H in lakes with contrasting residence
713 times. Paleoceanography and Paleoclimatology, 35(7), p.e2020PA003886.
714 Tierney, J.E., Russell, J.M., Huang, Y., Damsté, J.S.S., Hopmans, E.C. and Cohen, A.S., (2008).
715 Northern hemisphere controls on tropical southeast African climate during the past
716 60,000 years. *Science*, *322*(5899), pp.252-255.
717 Tierney, J.E., Russell, J.M., Damsté, J.S.S., Huang, Y. and Verschuren, D., (2011). Late
718 Quaternary behavior of the East African monsoon and the importance of the Congo Air
719 Boundary. *Quaternary Science Reviews*, *30*(7-8), pp.798-807.
720 Tierney, J.E., Pausata, F.S. and deMenocal, P.B., (2017). Rainfall regimes of the Green Sahara.
721 Science advances, 3(1), p.e1601503.
722 Tipple, B.J., Berke, M.A., Doman, C.E., Khachaturyan, S. and Ehleringer, J.R., (2013). Leaf-
723 wax n-alkanes record the plant–water environment at leaf flush. *Proceedings of the*
724 *National Academy of Sciences*, *110*(7), pp.2659-2664.

Wang, Z., Liu, H. and Cao, Y., (2018). Choosing a suitable εw-p by distinguishing the dominant plant sources in sediment records using a new Pta index and estimating the paleo-δDp spatial distribution in China. *Organic Geochemistry*, *121*, pp.161-168.

Xia, Z.H., Xu, B.Q., Mügler, I., Wu, G.J., Gleixner, G., Sachse, D. and Zhu, L.P., (2008). Hydrogen isotope ratios of terrigenous n-alkanes in lacustrine surface sediment of the Tibetan Plateau record the precipitation signal. *Geochemical Journal*, *42*(4), pp.331-338.

Yang, H. and Huang, Y., (2003). Preservation of lipid hydrogen isotope ratios in Miocene lacustrine sediments and plant fossils at Clarkia, northern Idaho, USA. *Organic Geochemistry*, *34*(3), pp.413-423.

734 Figures:

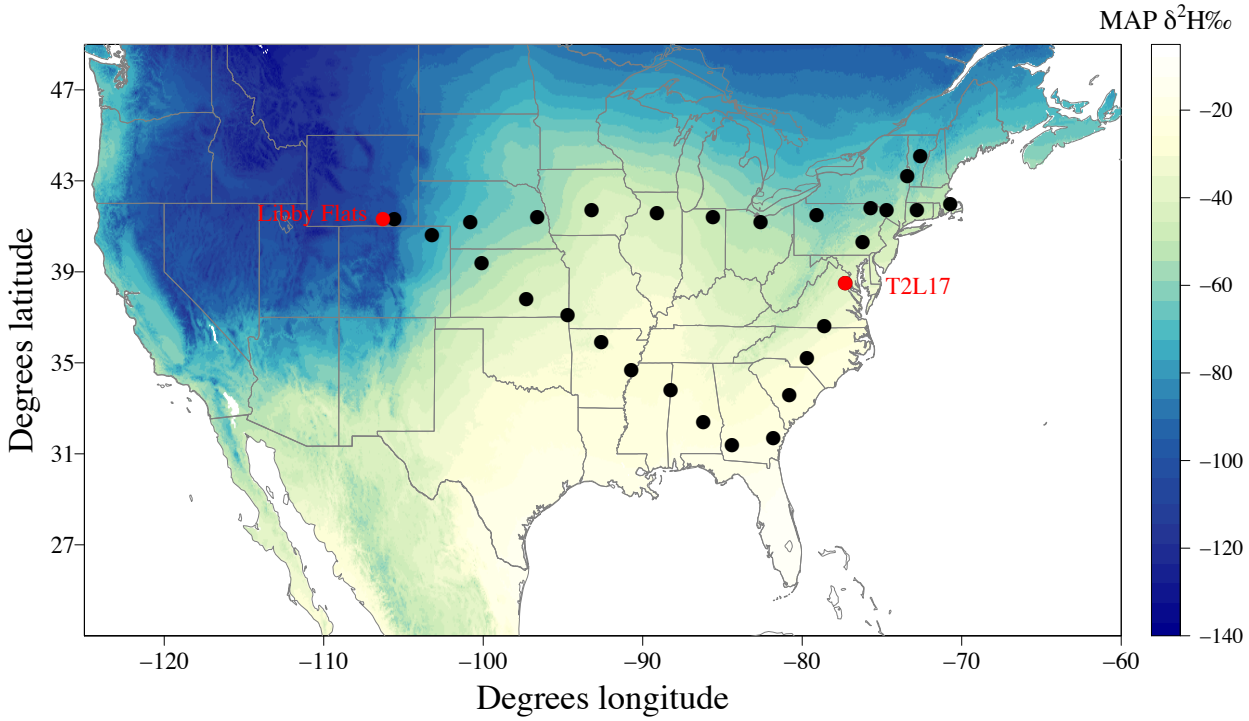

735 **Figure 1.** Map showing the site locations for plant and surface sediment collection (black
736 points), including Libby Flats Pond and Lake T2L17 (red points), which represent extremes with
737 respect to local gymnosperm and angiosperm vegetation respectively. Color scale displays
738 modeled δ^2H (‰) of mean annual precipitation (MAP) retrieved from
739 http://www.waterisotopes.org (Bowen, G. J., 2020).

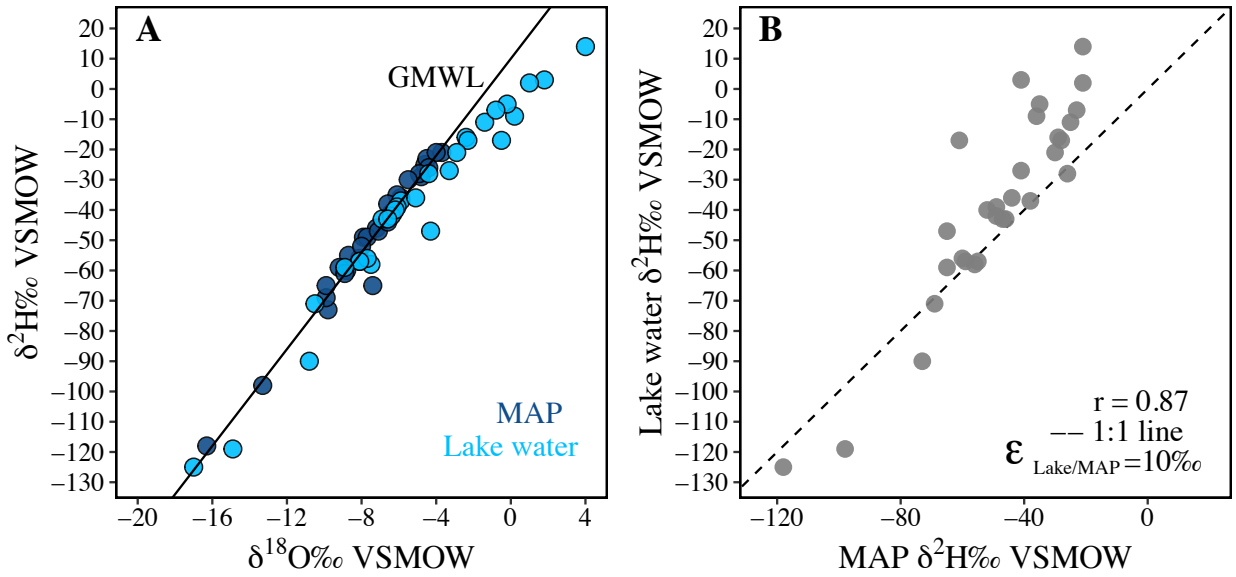

Figure 2. A. δ^2H versus $\delta^{18}O$ of measured lake water (light blue circles) show evidence of modest evaporative enrichment at some lakes compared to modeled mean annual precipitation (MAP, dark blue circles). Both values for each of our sites is plotted with respect to the global meteoric water line (GMWL, black line). **B.** The difference appears as positive departures from the 1:1 line (dashed) on a plot of lake water δ^2H versus modeled MAP δ^2H at each lake. The Pearson's correlation coefficient (r) and the mean epsilon value representing the offset between lake water δ^2H and MAP are shown in panel B.

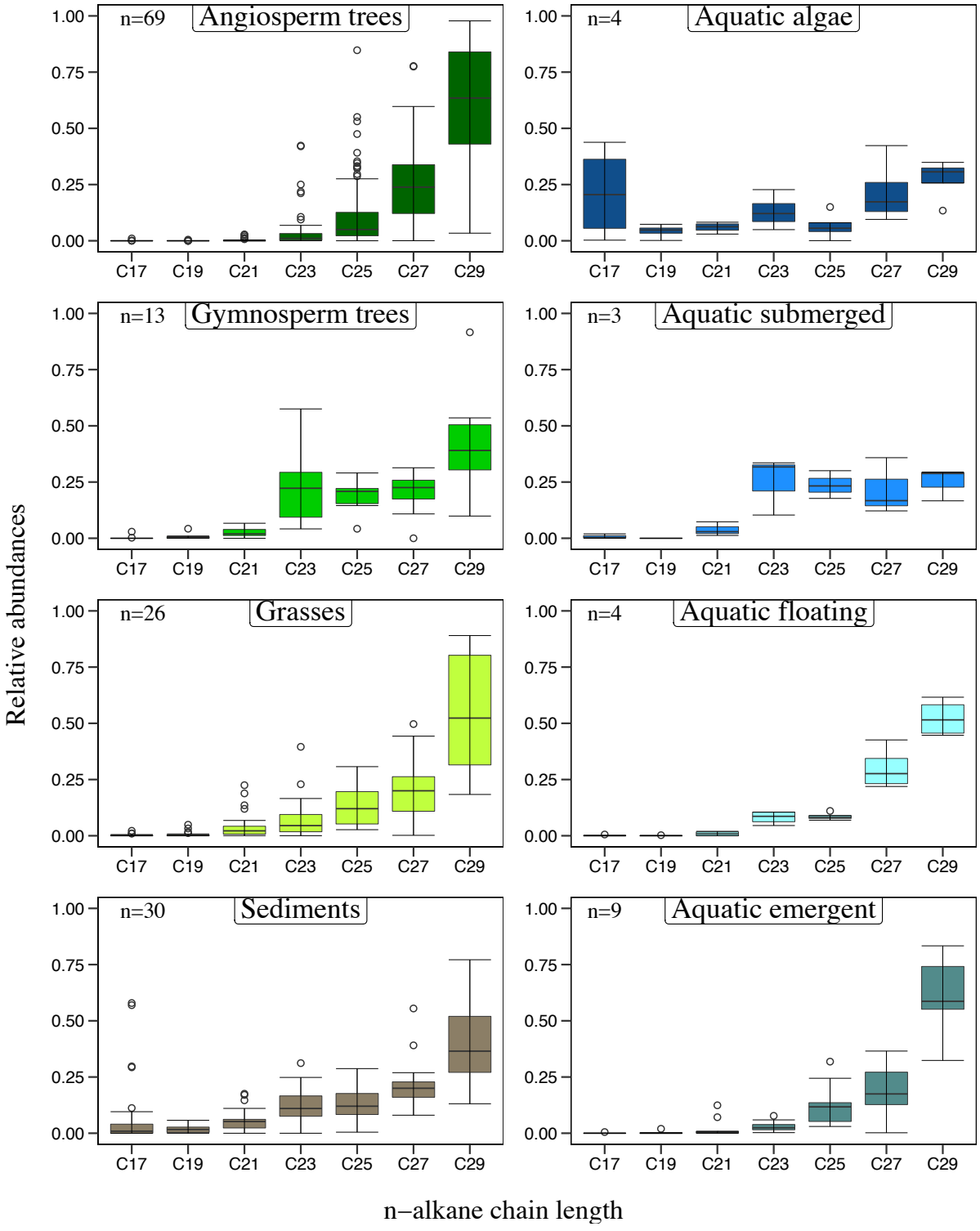

Figure 3. The relative abundances of leaf-wax n-alkanes in plants and sediments. Boxplot statistics are as follows: lower whisker represent the lowest value; lower hinge, the first quantile; middle hinge, the median; upper hinge, third quantile; and upper whisker, the highest value. Points represent outliers. Boxplots are colored coded to emphasize the sediments and the different plant groups.

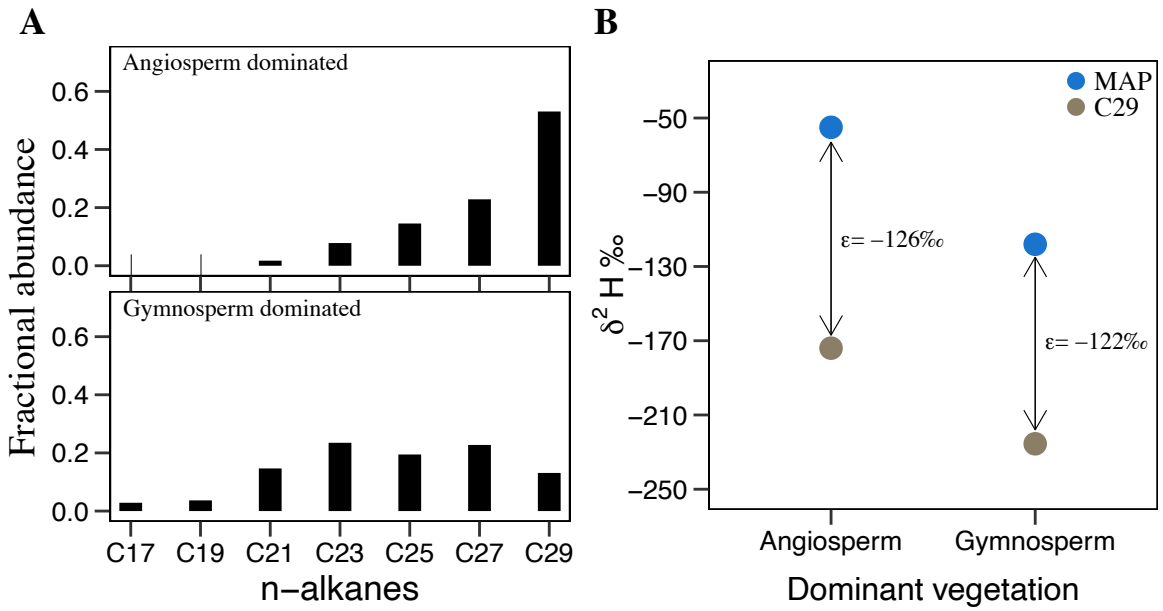

752 **Figure 4. A.** Fractional abundances of n-alkanes C17-C29 in lake sediments highlight
753 differences between an angiosperm-dominated site (T2L17) and a gymnosperm-dominated site
754 (Libby Flats), which are shown as red circles in Fig. 1. **B.** Despite the different distributions of
755 compounds and different potential sources, the net apparent fractionation factors (arrows)
756 between the δ^2H of alkane C29 (gray circles) and MAP (blue circles) are similar at the two sites.

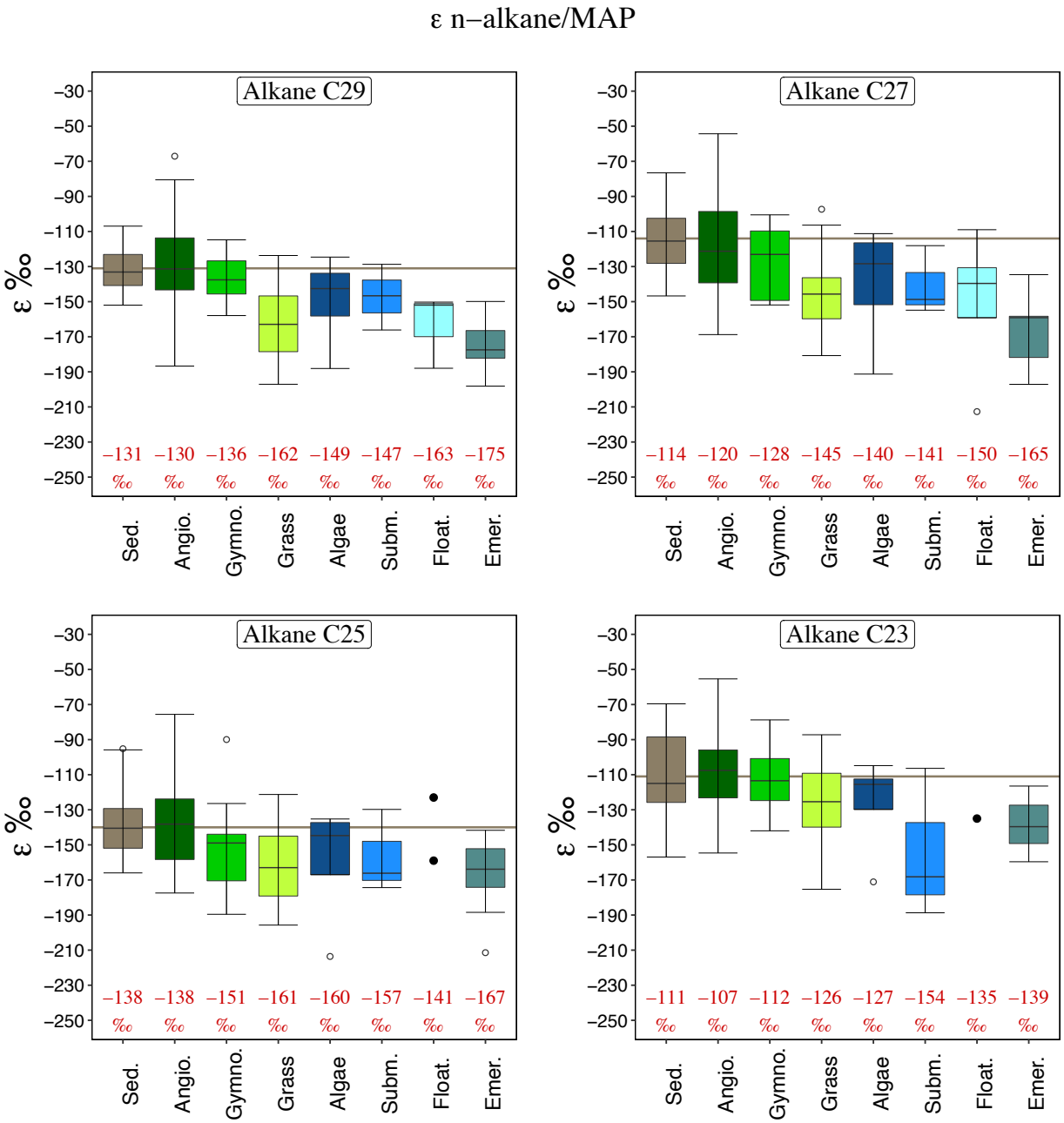

Figure 5. Distributions of the apparent fractionation (ε_{app}) between n-alkanes and MAP δ^2H‰ values for sediments and different plant types (color-coded as in Fig.2) for alkanes C_{23}-C_{29}. Horizontal lines represent the mean ε_{app} value between sediments and MAP (ε sediment/MAP) for each n-alkane while the mean ε_{app} value for each distribution is shown in red. Boxplot statistics are as follows: lower whisker = lowest value, lower hinge = first quantile, middle hinge = second quantile (median), upper hinge = third quantile and upper whisker = highest value. Open circles represent outlier data and black filled circles represent actual data points.

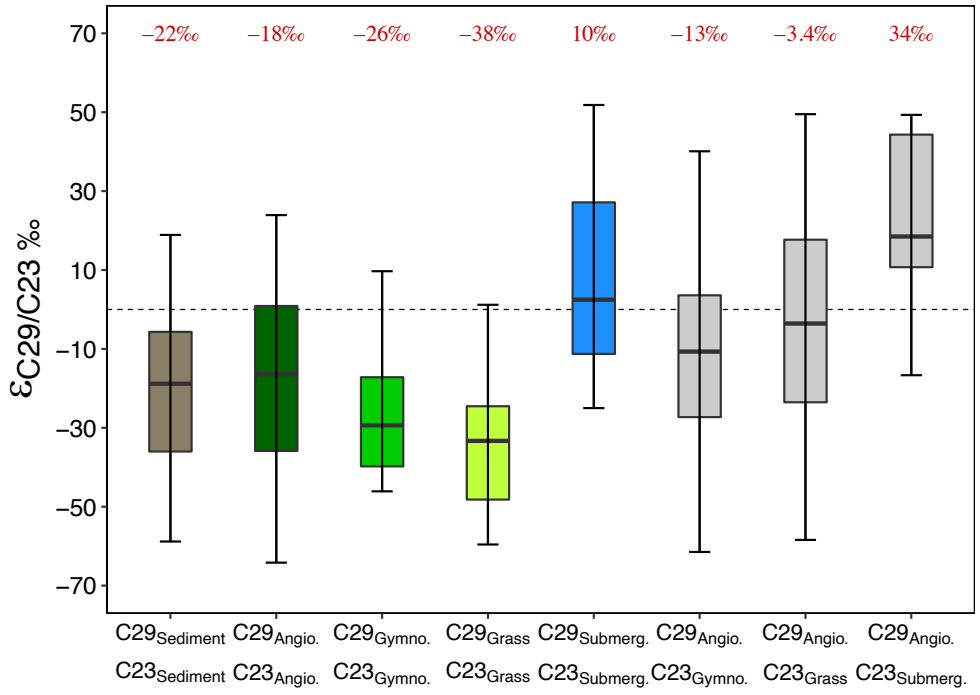

Figure 6. Distributions showing the δ^2H‰ differences ($\varepsilon_{C29/C23}$) between alkanes C_{29} and C_{23} in sediments and within plant groups (colored boxplots) and between a constant angiosperm source of alkane C_{29} and varying sources of alkane C_{23} (grey boxplots). Horizontal dashed line plotted at $\varepsilon_{C29/C23}$=0.

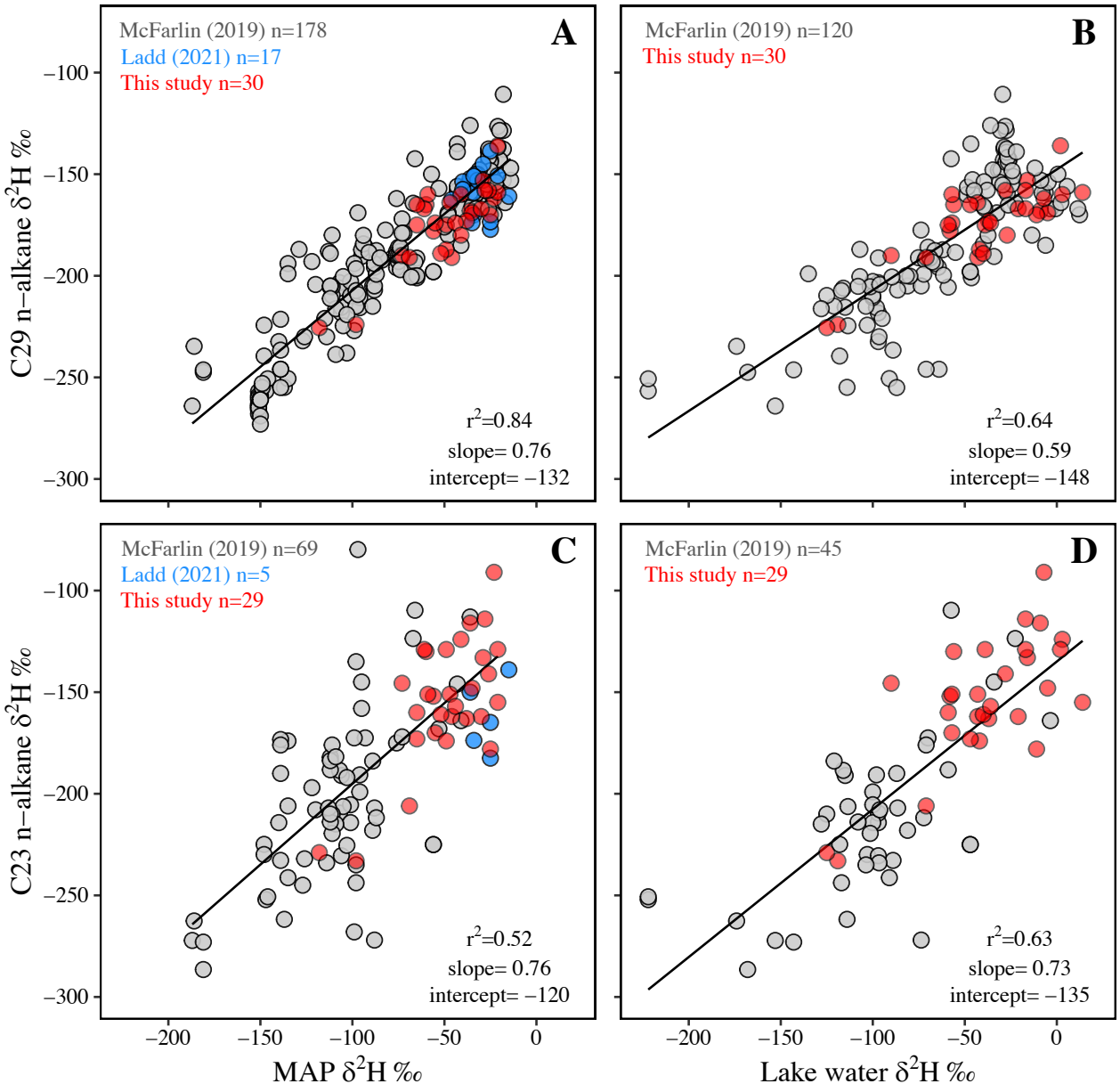

Figure 7. Scatterplots showing the global relationships between modeled MAP and measured lake water δ2H‰ values versus sediment alkane C29 and alkane C23 δ^2H‰ values. Compiled global δ^2H‰ data for lake water, modeled MAP, alkane C29 and alkane C23 were obtained from McFarlin et al., (2019) and Ladd et al., (2021) and are shown in gray and blue respectively; this study δ^2H‰ data are shown in red. All the relationships are statistically significant ($p<0.05$).

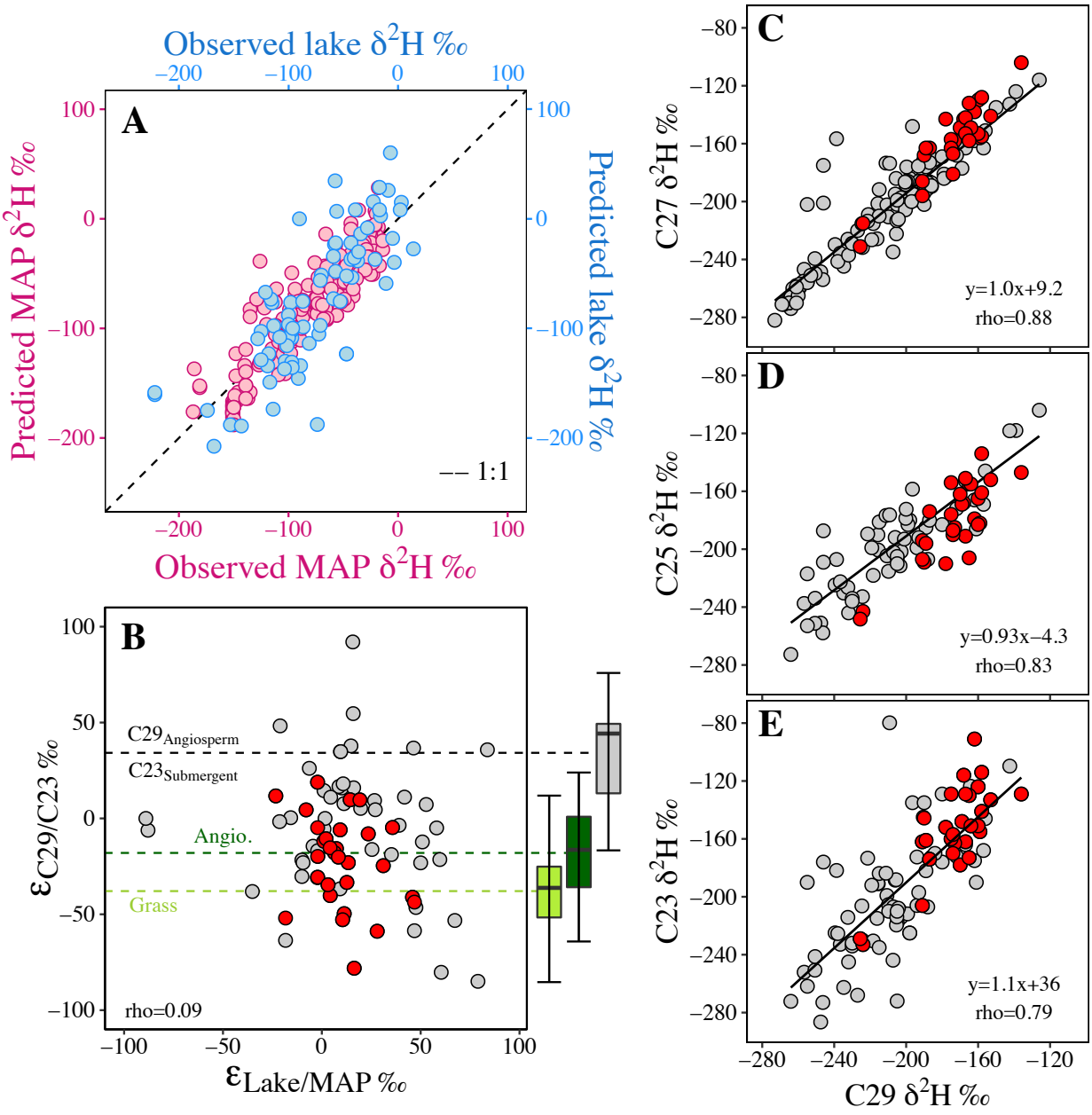

Figure 8. A. Scatterplot showing the observed versus predicted MAP based on alkane C_{29} (red, n=208) and the observed versus predicted lake water based on alkane C_{23} (blue, n=74); prediction uncertainties represent ± RMSE values for each model; the 1:1 line is shown in black. **B.** Apparent fractionation between modeled MAP and lake water (ε MAP/lake) versus the apparent fractionation between sediment alkane C_{29} and alkane C_{23} ($\varepsilon_{C29/C23}$) (n=74); box plots show the distribution of $\varepsilon_{C29angiosperm/C23submergent}$ (blue), $\varepsilon_{C29angiosperm/C23angiosperm}$ (dark green), and $\varepsilon_{C29grass/C23grass}$ (light green). Dashed lines represent the mean εC29/C23 of three distributions. **C-E.** Scatterplots showing the relationship between sediment alkane C_{29} and alkane C_{27} (n=115); alkane C_{25} (n=58); and alkane C_{23} (n=95). Statistically significant correlations are shown in red (rho, $p<0.05$). Data from this study is shown in red, from the global dataset compiled by McFarlin et al., (2019) is shown in grey, and from Ladd et al., (2021) is shown in blue.

784 **Table 1.** Site locations, environmental data and corresponding δ^2H‰ and $\delta^{18}O$‰ values of lake
785 water and modeled annual precipitation (MAP). δ^2H‰ and $\delta^{18}O$‰ values are reported relative to
786 VSMOW.

Lake	Latitude degrees	Longitude degrees	Elevation meters	MAT °C	MAP mm/yr	δ^2H‰ lake	$\delta^{18}O$‰ lake	δ^2H‰ MAP	$\delta^{18}O$‰ MAP
T1L9	31.39	-84.4	54	19.2	1300	14	4	-21	-3.7
Fishing	31.67	-81.81	11	19.5	1229	2	1	-21	-4
T1L8	32.35	-86.21	87	18.2	1287	-7	-0.8	-23	-4.5
Turkey Hill	33.55	-80.85	73	17.8	1202	-28	-4.4	-26	-4.4
Lamar	33.78	-88.27	110	16.5	1431	-11	-1.4	-25	-4.6
Bear Creek	34.71	-90.69	80	16.3	1302	-16	-2.4	-29	-4.8
Wheatfield	35.17	-79.68	169	15.9	1170	-17	-2.3	-28	-4.9
Ferguson	35.88	-92.63	473	14.1	1175	-5	-0.2	-35	-6.1
Buffalo	36.62	-78.58	12	14.5	1108	-21	-2.9	-30	-5.5
Spring	37.06	-94.73	245	14.4	1153	-9	0.2	-36	-5.9
T1L3	37.77	-97.32	405	13.7	878	3	1.8	-41	-6.4
Locust Shade	38.54	-77.35	45	13.6	1040	-37	-5.9	-38	-6.6
Antelope	39.37	-100.11	725	10.2	392	-58	-7.5	-56	-8.1
Middle Creek	40.27	-76.23	175	11.4	1139	-39	-6.1	-49	-7.9
Cody Pond	41.15	-100.75	852	9.6	523	-47	-4.3	-65	-7.4
Norwalk	41.23	-82.58	244	9.9	966	-40	-6.2	-52	-8
Labonte Pond	41.32	-105.59	2181	5.4	353	-119	-14.9	-98	-13.3
Eagle	41.44	-85.57	275	9.8	954	-43	-6.6	-47	-7.1
Cottonwood	41.45	-96.57	370	10.2	773	-17	-0.5	-61	-8.9
Beaver Meadows	41.52	-79.11	523	7.3	1165	-59	-8.9	-65	-9.9
Mendota	41.56	-89.13	235	9.5	928	-36	-5.1	-44	-6.6
Overland	40.62	-103.18	1200	10.2	392	-90	-10.8	-73	-9.8
T2L17	41.70	-74.69	479	7.7	1224	-57	-8.1	-55	-8.7
Quarry Spring	41.69	-93.24	241	10.1	908	-27	-3.3	-41	-6.3
Batterson	41.71	-72.79	94	10	1248	-42	-6.4	-49	-7.7
Blanding	41.8	-75.68	454	7.6	1127	-57	-8.1	-59	-9.2
Arms House	41.95	-70.66	24	10.2	1302	-43	-6.9	-46	-7.2
Carter's Pond	43.16	-73.42	151	7.9	1056	-56	-7.7	-60	-8.8
Twin Ponds	44.06	-72.58	410	5.5	1057	-71	-10.5	-69	-9.9
Libby Flats	41.32	-106.29	3192	0.1	1014	-125	-17	-118	-16.3

Table 2. Pearson correlations values between predicted MAP and predicted seasonal δ^2H‰ values and between MAP and measured lake water δ^2H‰ values (n=29). All correlations are significant ($p<0.05$).

Variable	MAP	Lake water
DJF	0.92	0.81
MAM	0.97	0.88
JJA	0.94	0.86
SON	0.93	0.71

Table 3. Apparent fractionation factors between n-alkanes δ^2H‰ values and modeled annual precipitation and lake water δ^2H‰ values in sediments and different plant types (ε wax/MAP, ε wax/lake).

	ε wax/MAP				ε wax/lake			
Type	**C29**	**C27**	**C25**	**C23**	**C29**	**C27**	**C25**	**C23**
Angiosperm trees	-130±21‰ n=66	-120±24‰ n=63	-138±23‰ n=61	-107±24‰ n=32	-	-	-	-
Gymnosperm trees	-136±14‰ n=13	-128±21‰ n=12	-151±27‰ n=13	-112±21‰ n=12	-	-	-	-
Grass	-162±23‰ n=26	-145±22‰ n=26	-161±23‰ n=26	-126±22‰ n=22	-	-	-	-
Algae	-149±28‰ n=4	-140±36‰ n=4	-160±37‰ n=4	-127±30‰ n=4	-163±19‰ n=4	-154±29‰ n=4	-173±30‰ n=4	-140±28‰ n=4
Submergent	-147±19‰ n=3	-141±20‰ n=3	-157±24‰ n=3	-154 ± 43‰ n=3	-156±23‰ n=3	-150±24‰ n=3	-166±28‰ n=3	-164±47‰ n=3
Floating	-163±21‰ n=3	-150±44‰ n=4	-141±26‰ n=2	-135‰ n=1	-163±20‰ n=3	-154±43‰ n=4	-141±29‰ n=2	-137‰ n=1
Emergent	-175±15‰ n=9	-165±21‰ n=9	-167±23‰ n=8	-139±16‰ n=6	-179±15‰ n=9	-169±23‰ n=9	-171±30‰ n=8	-140±19‰ n=6
Sediment	-131±12‰ n=30	-114±17‰ =29	-138±20‰ n=29	-111±24‰ n=29	-140±18‰ n=30	-123±19‰ =29	-147±21‰ n=29	-119±24‰ n=29